Chaos, Solitons and Fractals 172 (2023) 113565

Contents lists available at ScienceDirect

Chaos, Solitons and Fractals

journal homepage: www.elsevier.com/locate/chaos

Complex dynamics of the simplest neuron model: Singular chaotic Shilnikov attractor as specific oscillatory neuron activity

N.V. Stankevich [a,*], A.S. Gonchenko [a,b], E.S. Popova [a], S.V. Gonchenko [a,b]

[a] Laboratory of Topological Methods in Dynamics, National Research University Higher School of Economics, Bolshaya Pecherskaya str., 25/12, Nizhny Novgorod 603155, Russia

[b] Scientific and Educational Mathematical Center "Mathematics of Future Technologies", Lobachevsky State University of Nizhny Novgorod, 23 Prospekt Gagarina, Nizhny Novgorod 603950, Russia

ARTICLE INFO

Keywords:
Neuron model
Chialvo map
Endomorphism
chaos
Singular Shilnikov attractor
Snap-back repeller

ABSTRACT

We study complex dynamics of the Chialvo model that is the simplest neuron-type model in form of a four-parameter family of two-dimensional noninvertible maps (endomorphisms). Main elements of bifurcation diagram in the plane of two parameters have been constructed in which regions corresponding to both quasi-periodic and chaotic oscillations are selected. We also indicate special regions corresponding to singular discrete chaotic Shilnikov attractors that we consider as a new type of the so-called snap-back repellers (over an unstable focus). The study of time series was carried out in which there were classified patterns of specific oscillatory activities in the cases when homoclinic orbits to the unstable focus exists and, when such orbits were not yet formed but a strange attractor already exists. New dynamical characteristics are proposed, with the help of which it is possible to assess the level of distinctness of atypical oscillatory activity.

1. Introduction

Neuron models are one of the most important objects in neurophysiology, neurodynamics, machine learning, nonlinear dynamics, etc. [1–4]. These models are used as a basis for modeling various real-life applications of wide rang: from investigation of isolated (single) cell till modeling of brain functioning. There are a large number of models with their own specifics. Note that the study of features characteristic of one model is very important, since they can manifest themselves in the dynamics of complex networks of interacting such or similar models.

The important class of neuron models is represented by a single neuron models functioning in accordance with the Hodgkin-Huxley formalism [2,5,6]. The first model was proposed by Hodgkin and Huxley; it was presented as a system of four ordinary nonlinear differential equations and demonstrated all the types of character behavior of such systems: a stable equilibrium state, spike and burst oscillations [6]. Later it was shown that the minimal mathematical model supporting such properties can be three-dimensional flow dynamical system, such as the well-known Hindmarsh-Rose model [7,8], the Sherman-Rintzel model [9,10], the reduced leech neuron model [11,12] and etc. The mathematical model can also be written as a dynamical system with discrete time, so called map. For a map, the time in the model is discrete, which is good, since in experiments the time of observation and analysis are also usually discrete. So when recording experimental data, for example, an EEG signal, we always have a set of discrete data, in accordance with the sampling step. Therefore, using maps for modeling continuous processes is justified, while it allows simplifying the model as much as possible due to the reduction of the phase space dimension. The simplest neuron model in form of a map should have two dynamical variables, one of which is responsible for the fast time scale and the other for the slow one. Many different models of neurons in the form of maps of different dimensions are also well known in the literature [13–15].

In the present paper we deal with numerical simulation of the dynamics of the Chialvo map, which was first introduced in [16]. This map was studied by various authors and used as an object for certain numerical experiments [16–20]. At the same time, in many papers focused on features of networks in applied problems, exactly the same parameters were used that were proposed in [16]. However, as far as we know, when studying bifurcation scenarios and dynamical regimes, a detailed analysis of the attractors that arises here has not been carried out.

Among these attractors, the Shilnikov attractors are of particular interest. In the case of multidimensional flows, such attractors were introduced in [21], where a universal scenario for their occurrence in one-parameter families was also proposed. Such an attractor contains a

* Corresponding author.
E-mail address: stankevichnv@mail.ru (N.V. Stankevich).

https://doi.org/10.1016/j.chaos.2023.113565
Received 23 February 2023; Received in revised form 26 April 2023; Accepted 10 May 2023

saddle-focus equilibrium and entirely its two-dimensional unstable manifold. In [22,23] this scenario was generalized to the case of discrete Shilnikov attractors of three-dimensional maps—such attractors contain a fixed (periodic) point that is a saddle-focus with a two-dimensional unstable manifold (this point has eigenvalues $\lambda_{1,2} = \gamma e^{\pm i\psi}$, $\lambda_3 = \nu$, where $\gamma > 1$, $|\nu| < 1$, $\nu \neq 0$, $|\nu\gamma^2| < 1$). All these attractors are strange because they satisfy the Shilnikov criterion from [24] and, therefore, contain non-trivial hyperbolic subsets.

In his famous work [25] F.R. Maroto showed that multidimensional noninvertible maps can possess chaotic attractors containing completely unstable periodic orbits (which have all eigenvalues exceed 1 in magnitude). Such attractors are called snap-back repellers. By now, many examples of attractors of such type are known. In particular, in the works [26,27] by L. Gardini it was shown that two-dimensional non-invertable maps can posses spiral snap-back repellers. They contain a fixed point that is an unstable focus type (with eigenvalues $\gamma e^{\pm i\psi}$, where $\gamma > 1$) and, nevertheless, are attractors due to the possibility for some points of phase plane to immediately jump directly into the unstable focus under one iteration of the map. Such virtually fixed (periodic) point can be *homoclinic*. Let O be the unstable focus, P be a point such that $P \neq O$ and $f(P) = O$. Then the point P is homoclinic to O, if there is a sequence $\ldots, p_{-i}, p_{-i+1}, \ldots, p_{-1}, P$ of points such that $p_{-i+1} = f(p_{-i})$, $f(p_{-1}) = P$, $f(P) = O$ and $p_{-i} \to O$ as $i \to \infty$. Of course, diffeomorphisms do not have such instantly homoclinic points: any homoclinic point of a diffeomorphism tend to a fixed (periodic) orbit as result of infinitely many both forward and backward iterations. Thus, homoclinic dynamics in the cases of diffeomorphisms and endomorphisms are rather different. Nevetheless, as we show in this paper, they have many common. In particular, in this paper we consider attractors, which we call two-dimensional *singular Shilnikov attractors* or, in traditional terminology of noninvertable maps, spiral snap-back repeller, and show that there exist certain analogy with both spiral (Shilnikov) attractors in three-dimensional slow-fast systems, like the Rössler system [28,29], the Nikolis-Gaspard model of chemical oscillator [30], and discrete Shilnikov attractors of three-dimensional diffeomorphisms, see e.g. [22,23,31].

It is obvious that the dynamics of 2D noninvertible maps is much more complicated than ones for 2D diffeomorphisms. For example, the latter can not have attractors containing completely unstable periodic orbits (periodic sources). At that time, such attractors, the so-called snap-back repellers [24,32], are well-known in 2D endomorphisms, see e.g. [26,27,33–35]. In the paper we show how such attractor containing a repelling focus can appear in parameter families of Chialvo maps as result of a bifurcation scenario that is similar in a sense to the scenario of emergence of discrete Shilnikov attractor in 3D diffeomorphisms. In any case, main steps of both scenarios are similar: a stable periodic orbit → Andronov-Hopf bifurcation and creation of new attractor – a stable invariant curve → break-down of this curve and all proper (visible) stable invariant subsets and a formation of a homoclinic orbit to the initial periodic orbit (a saddle-focus for 3D case and a repelling focus for 2D case).

Nevertheless, despite these analogs, scenarios for 2D-noninvertible and 3D-invertible cases can look as completely different. First of all, this relates to different mechanisms for break-down of invariant curves and for formation of homoclinic dynamics. We discuss this in Section 3.

Such feature of attractors like Shilnikov attractors can manifest themselves by special uncharacteristic types of oscillatory activity, see e.g. [36] where an example of such specific time series was shown at formation of the Shilnikov attractor in the Rosenzweig–MacArthur model.

In the paper we study a possibility of the emergency of an attractor with similar properties, but for a two-dimensional noninvertible map - the Chialvo model that is the simplest model of a neuron in the form of a map. Such an attractor, by analogy with the three-dimensional case, we call a singular discrete Shilnikov attractor, and in the standard terminology of noninvertible maps, it is a snap-back repeller (of spiral type). In the parameter space of the model, we localize areas with complex dynamics, identify special types of chaotic attractors, and discuss scenarios for their development. We also analyze the time series generated by the map and offer some dynamical characteristics that can be used to study special patterns in the time series.

The work is structured as follows. In Section 2 we present the map and analyze the structure of its parameter space. In Section 3 we discuss the features of the chaotic attractors observed in this map, including chaotic attractors arising as a result of cascades of period doubling bifurcations and scenarios of invariant curve break-down, and also give a brief description of the Shilnikov discrete attractor with describing the formation of the Shilnikov singular attractor associated with the snap-back repeller mechanism in the Chialvo model. In Section 4 we present the results of analysis of time series in the model, determine a special type of characteristic of dynamical behavior in the Shilnikov singular attractor, and calculate these characteristics.

2. Object of study: Chialvo map, parameter space, main bifurcations

The Chialvo model was proposed in [16] as the simplest map T in which one can observe burst-spike dynamics, including chaotic ones. The Chialvo map is written as follows:

$$\begin{aligned} x_{n+1} &= x_n^2 exp(y_n - x_n) + I, \\ y_{n+1} &= a y_n - b x_n + c. \end{aligned} \tag{1}$$

Here the variable x reproduces the dynamics of the membrane potential; y is a restoring variable; a, b, c, I are parameters. These parameters control the dynamics of the system as follows: a is the recovery time constant ($a < 1$); b determines the dependence of restorative processes on the level of activity; c is a constant offset; parameter I characterizes the action of ion currents injected into the neuron. Thus, model (1) is a two-dimensional map with four control parameters. Note that this map is an endomorphism, i.e. noninvertible map. The Jacobian matrix of map (1) can be written as follows:

$$\widehat{I} = \begin{vmatrix} (2x - x^2)exp(y - x) & x^2 exp(y - x) \\ -b & a \end{vmatrix} \tag{2}$$

Then the Jacobian will be:

$$J = x(2a - x(a - b))exp(y - x). \tag{3}$$

Note, that the Jacobian is independent of the parameters c and I and can vanish, namely,

$$J = 0 \to x = 0 \cup x = \frac{2a}{a - b}. \tag{4}$$

This means that map (1) is noninvertible. Moreover, it folds R^2 twice. First, it maps R^2 into the half plane $D_1 : x \geq I$ that is positively invariant, i.e. $T(D_1) \subset D_1$. Second, T folds D_1 along the line $x = \frac{2a}{a-b}$, which allows to realize "snap-back" dynamics in T also for $I > 0$. This property is important for this map, we will discuss this feature later.

It was shown in [16] that at $a = 0.89$, $b = 0.18$, $c = 0.28$, $I = 0.03$ the chaotic burst-spike behavior is observed in map (1). To obtain a general view of the dynamics and their bifurcations, we fixed the values of a and b close to those: $a = 0.9$, $b = 0.2$, and consider the other two parameters c and I to be control ones.

Let us study the bifurcation structure of the (c, I) parameter plane, as well as the basic dynamical regimes and bifurcations of Chialvo map (1). For this analysis, we constructed a chart of dynamical regimes (Fig. 1a), a two-parameter bifurcation diagram (Fig. 1b), and a chart of maximal amplitudes (Fig. 1c). On the chart of dynamical regimes (Fig. 1a), parameter values corresponding to periodic orbits with a period of up to 120 are distinguished (they are painted in different colors in accordance with the palette in Fig. 1a). If a number of observed points in a regime is >120, then we do not distinguish it from non-periodic (chaotic) one and

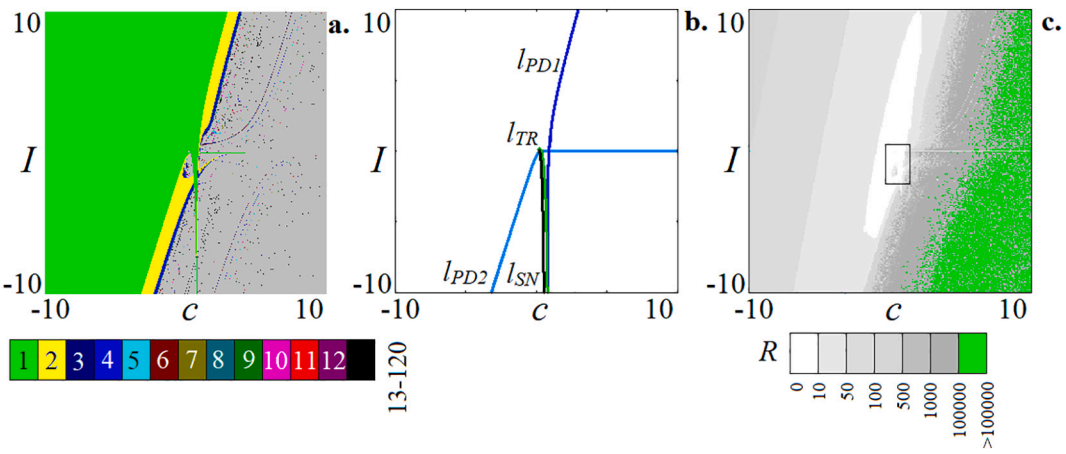

Fig. 1. Parameter plane analysis for Chialvo map (1) at $a = 0.9$, $b = 0.2$. a. Chart of dynamic regimes; b. Two-parameter bifurcation diagram; c. Chart of maximum amplitudes.

the corresponding pixel of the parameter plane is assigned the gray color. The two-parameter bifurcation diagram (Fig. 1b) was obtained using the XPPAUT numerical bifurcation analysis package [37]. It demonstrates the bifurcation for fixed points:

- period-doubling bifurcation lines (blue color);
- Neimark-Sacker bifurcation lines (green color), as a result of which a stable fixed point is transformed into an unstable focus, and a stable invariant curve is born;
- saddle-node bifurcation line (black), which corresponds to the birth of a pair of fixed points (stable node and saddle or unstable node and saddle).

Note that map (1) has such regimes in which the orbits first go far enough from the region of observation in the phase space, to a distance R, and then return to this region. To detect such regimes, we build in the plane of (c, I)-parameters the so-called chart of maximal amplitudes (Fig. 1c), on which regions corresponding to different maximums of R are colored with different shades of gray (according to the palette below). When constructing this diagram, both coordinates x and y were taken into account, and R was calculated according to the following rule:

$$\begin{aligned} R &= max(R_n), \\ R_n &= \sqrt{x_{n^2} + y_{n^2}}, \quad n = 0, 1, \ldots, N, . \end{aligned} \tag{5}$$

where N is the number of iterations during R was determined, in our experiments $N = 2500$.

The chart of dynamical regimes (Fig. 1a) clearly shows the basic types of dynamical regimes. The green-colored part of the chart corresponds to the region where the fixed point is stable. As the parameter c increases, period-doubling bifurcation and a further cascade of doublings with the formation of chaotic dynamics are observed. In the vicinity of zero values of the parameters c and I, a rather complex structure is observed: long "offshoots" of the stability regions of the stable fixed point are visible, which stick into other regions (where, for example, period doublings and chaos are observed). The bifurcation diagram (Fig. 1b) makes it possible to understand also that the intersection of two "offshoots" corresponds to the intersection of the period doubling lines of two different fixed points.

For map (1) it is not possible to obtain analytical expressions for fixed points, while it can have one, two or three fixed points [16,17,19]. The fixed points are determined from the following equations:

$$\begin{aligned} x_0 &= x_0^2 exp\left[\frac{-x_0(b-a+1)}{1-a} + \frac{c}{1-a}\right] + I, \\ y_0 &= \frac{-bx_0 + c}{1-a}. \end{aligned} \tag{6}$$

With fixed values of the parameters a and b ($a = 0.9$ and $b = 0.2$), one can obtain a transcendental equation that determines the coordinates of fixed points (x_0, y_0). The function corresponding to this equation has the following form:

$$F(x) = x^2 exp(-3x) exp(10c) - x + I. \tag{7}$$

It is clearly seen that the parameter I does not change the form of the function (7), but shifts it along the ordinate axis. The parameter c changes the function itself and the number of bends on it, which can change the number of fixed points in map (1).

Fig. 2 shows the plots of the function (7) for $I = 0$. Fig. 2a presents the function at $c = 0$. It can be seen from (7) that there is a root at the point $x_0 = 0$. In this case, as $x \to +\infty$, we can determine asymptotic behavior of functions: $x^2 \to +\infty$, $exp(-3x) \to 0$. The exponent function decreases much faster than the quadratic function, so their product vanishes and for positive x_0 we see a close to linear dependence $F(x)$. For negative values of x: at $x \to -\infty$, we have $x^2 \to +\infty$, $exp(-3x) \to +\infty$. Both functions increase and we see a non-linear increase in the plot. For fixed nonzero values of c the graph of function $F(x)$ will change as follows. For $c < 0$, the factor exp(10c) is small (exponentially small in c) and, therefore, an interval of values of x where function $F(x)$ will be close to linear one expands to negative values of x (the more $|c|$ the longer), see Fig. 2b. Thus, for $c < 0$, additional bends do not appear and the fixed point remains the only one.

For c > 0, the character of the function changes (Fig. 2c). The factor exp(10c) is monotonically increasing, and for small values of x its contribution becomes greater than that for exp(-3x). Thus, in Fig. 2c we see the formation of a local maximum, and, accordingly, the birth of two new fixed points.

For $I = 0$ the equation $F(x) = 0$ reads as $x(x \exp(-3x) \exp(10c) - 1) = 0$. Thus, the root $x = 0$ exists always. Other roots can be found from the equation $f(x) = x \exp(-3x) \exp(10c) = 1$. The function $f(x)$ is negative for $x < 0$ and tends to 0 as $x \to +\infty$. It has global maximum at $x = 1/3$ and $f(1/3) = 1/3 \exp(-3x) \exp(10c)$. Then $f(1/3) = 1$ when $\exp(10c-1) = 3$, i.e. for $c = c^* = \frac{ln3-1}{10}$. Thus, map (1) with $I = 0$ has one fixed point at $c < c^*$, one more fixed point (a saddle-node) appears at $c = c^*$, and three fixed points exist at $c > c^*$.

A similar one-parameter analysis can also be carried out numerically using the XPPAUT software package. Fig. 3a shows a one-parameter diagram for the fixed point, characteristic for positive values of the

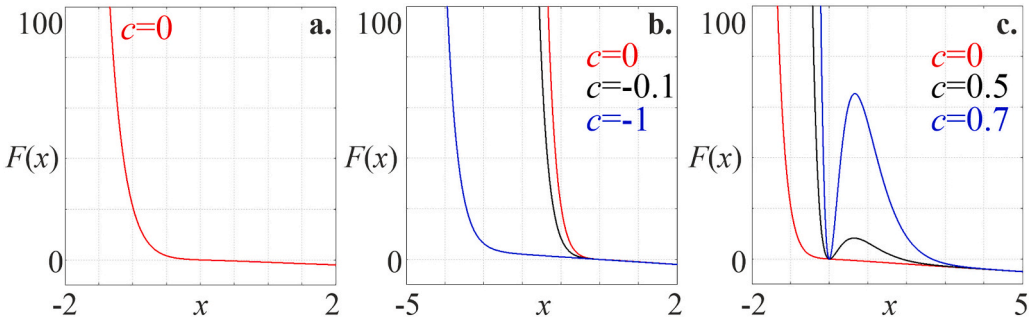

Fig. 2. Plots of the function (7), which determines the coordinates of the fixed points of the Chialvo map at $I = 0$. a. $c = 0$; b. $c \leq 0$; c. $c \geq 0$.

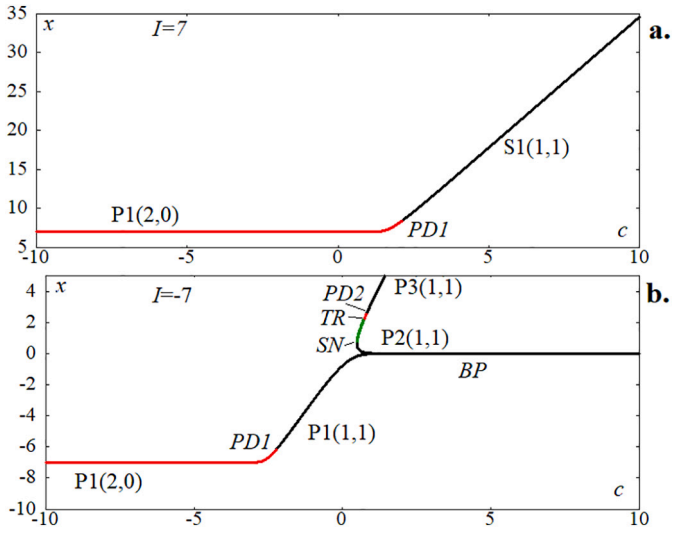

Fig. 3. One-parameter bifurcation diagrams for fixed points of the Chialvo map (1), $a = 0.9$, $b = 0.2$. a. $I = 7$; b. $I = -7$. The red line is a stable fixed point P(2,0), the black line is a saddle fixed point P(1,1), the green line is an unstable fixed point P(0,2). (For interpretation of the references to color in this figure legend, the reader is referred to the web version of this article.)

parameter I, at $I = 7$. The stable fixed point P(2,0) is marked in red. To denote the type of a point, we will use the indices in brackets corresponding to the dimensions of their stable and unstable manifolds. Saddle points with a one-dimensional stable and one-dimensional unstable manifold, P(1,1), and unstable points with two-dimensional unstable manifold P(0,2) we depict in one-parametr bifurcation diagram with black and green color, respectively. It is clearly seen that in this case ($I > 0$) there is only one fixed point. For negative values of the parameter c, we see that the coordinate of the fixed point is close to constant depending on the parameter c and is determined by the parameter I, i.e. $x_0 \approx I$, which corresponds to the linear growth of the function (7). Then from (1) we can get an expression for the coordinate y_0:

$$x_0 \approx I \rightarrow y_0 \approx \frac{-bI + c}{1 - a}, \tag{8}$$

with $a = 0.9$, $b = 0.2$ we obtain: $y_0 \approx -2I + 10c$. Thus, for negative c, the coordinate y of the fixed point will be more 10 times than x variable. For positive values of the parameter c, the fixed point changes its value and begins to increase, then it undergoes a period doubling bifurcation, and in Fig. 3a we see further growth of the variable for the saddle point P1(1,1). As c increases, the fixed point undergoes a cascade of period doubling bifurcations (the line of the first doubling is shown in Fig. 1b in dark blue color, l_{PD1}).

For negative values of the parameter I, we also see the line of the period doubling bifurcation (l_{PD2}) on the bifurcation diagram, but it corresponds to another fixed point. Fig. 3b shows the one-parameter bifurcation diagram of model (1) for $I = -7$. The bifurcation diagram for $c < 0$ is similar to Fig. 3a, for large values of parameter c, the fixed point is defined as $x_0 \approx I$, while the variable y will not increase so intensively, because c and I with opposite signs are subtracted. As c increases, the period doubling bifurcation also occurs, however, further the growth of the variable stops and the branch of the bifurcation diagram for large positive c tends to $x_0 = 0$. At the same time, here one can observe a symmetry breaking bifurcation (BP), as a result of which the second branch of the saddle point P2(1,1) is born. The point P2(1,1) merges with the unstable node P3(0,2) as a result of the saddle-node bifurcation SN. With an increase in parameter c, the node transforms into a focus and then the point P3(0,2) undergoes a reverse Neimark-Sacker bifurcation, and in Fig. 2b we see a small region of existence of a stable fixed point P3(2,0), which then undergoes a period doubling bifurcation and turns into saddle P3(1,1). If we move in the opposite direction along the parameter c, then the saddle point P3(1,1) is observed in the map (1), as a result of the reverse period doubling bifurcation, the point becomes stable. Then it undergoes a Neimark-Sacker bifurcation and the birth of an invariant curve is observed. After that, the point P3(0,2) merges with the point P2(1,1) as a result of a saddle-node bifurcation. The indicated lines of saddle-node bifurcations and period doublings form the above-described "offshoots" in the chart of dynamical regimes (Fig. 1a). Thus, in the vicinity of zero values of the parameters (c, I), the parameter plane has a complex structure due to the appearance of three fixed points in the system, which we will consider in detail below.

The chart of maximal amplitudes presented in Fig. 1c demonstrates one of the interesting features of the Chialvo map dynamics. Dynamical variables of map (1) can reach enough big values, we can see vast areas with large values of the coefficient R determined in correspondence (5). Conventionally, areas with large values of dynamical variables can be divided into two groups: (i) where there is a fixed point; (ii) where oscillations are observed. The first region corresponds to the situation when the fixed point in at least one of the variables has a sufficiently large amplitude. The mechanism by which the growth of dynamical variables for fixed point is obtained, we described earlier, in accordance with (8).

The second case is more interesting, when oscillations are observed in the model, and one can see impulsive high-amplitude oscillations (random sequence of overshoots) for certain values of parameters. Such behavior is an interesting feature of model (1). With the help of such time series, it is possible to describe the specific behavior of neurons, the so-called extreme events, when the dynamical variable becomes large in amplitude [38–40]. In the framework of this paper, we would like to focus on the features of the system dynamics, where there are no high-amplitude pulses, or they are moderate. The region where the oscillation amplitude does not exceed 10 is localized in the vicinity of zero values of the parameter c and I and is indicated in Fig. 1c by a rectangle. Further we study this area in more detail.

Fig. 4 shows a zoomed fragment of the chart of dynamical regimes (Fig. 4a), the two-parameter bifurcation diagram (Fig. 4b) and a chart of Lyapunov exponents (Fig. 4c) demonstrating the structure of parameter plane in the vicinity of zero values of the parameters c and I. The chart of Lyapunov exponents was constructed as follows: the parameter plane was scanned with a small step, and for each point the spectrum of Lyapunov exponents was calculated, depending on the values of the exponents, the point on the parameter plane was painted in one color or another. In a two-dimensional endomorphism, four types of dynamical behavior depending on the values of the Lyapunov exponents are possible. Correspondence of the Lyapunov exponents signature, dynamical regime and color on the chart is presented in Table 1.

In Fig. 4b, the light purple color marks the area where three fixed points exist. This region is bounded by saddle-node bifurcation lines (black line l_{SN} and brown line l_{SNa}). The chart of dynamical regimes (Fig. 4a) clearly shows hard transitions between different dynamical regimes. This indicates the presence of multistability in the system, which is localized in the region of the parameter space, where there are three fixed points. “Offshouts” with a stable fixed point regime overlap with areas of other dynamical regimes. The mechanism of development of multistability can be understood by analyzing the bifurcation lines (Fig. 4b). Multistability with fixed points appear as a result of a saddle-node bifurcation marked in Fig. 4b by a black line (l_{SN}). Moreover, as a result of this bifurcation, a saddle point P2(1,1) and an unstable point P3 (0,2) are born. As the parameter c increases, the unstable focus becomes stable P3(2,0) as a result of the inverse Neimark-Sacker bifurcation (l_{TR}) and then undergoes a cascade of period doubling bifurcations. At the same time, in this region of parameters, one can observe a cascade of doublings and chaos resulting from doublings of the fixed point P1(2,0), thus forming multistability.

On the bifurcation diagram, the line of birth of the invariant curve is traced. The Lyapunov exponent chart allows to localize areas in the parameter space where an invariant curve exists, as well as to trace directions in the parameter space where the invariant curve destroys and chaotic dynamics is formed. Thus, two areas can be distinguished where invariant curves are observed, which are marked on the chart of Lyapunov exponents (Fig. 4c) by the symbols Q_1 and Q_2. The region Q_1 is located along the birth line of the invariant curve from the third fixed point P3(2,0). The domain Q_2 has a spot form and an invariant curve is generated on the base of the fixed point P1(2,0). On the basis of invariant curves in each region one can observe the development of chaos, the features of which we will consider in detail in the following Sections 3–4.

3. Variety of chaotic attractors

As shown above, chaotic behavior is formed in the parameter space in accordance with various bifurcation scenarios, as well as on the basis of various fixed points. In this Section 3, we consider in more detail the features of various chaotic attractors. We chose three routes in the parameter plane (c, I), shown in Fig. 4b. **Route A** passes through the region of multistability of periodic and chaotic attractors. **Route B** passes through the Q_2 quasi-periodic region and chaotic regimes. **Route C** passes through the Q_1 quasi-periodic region and goes into chaos.

3.1. Cascades of period doubling bifurcations

The simplest and most common scenario for chaos development in various maps is a cascade of period-doubling bifurcations of a fixed point.[1] This scenario is also observed in Chialvo map (1). It is easy to track this scenario for various fixed points in the chart of dynamical regimes (Fig. 1a) when varying the control parameters. Moreover, one can observe multistability between chaotic attractors born on the basis of different fixed points. This scenario of the development of chaos and multistability can be observed when passing along Route A on the parameter plane for a fixed value of parameter I: $I = -1.94$. Fig. 5 shows different illustrations of the chaotic attractors development in accordance with this scenario and multistability.

Fig. 5a and b show bifurcation trees built with inheritance of initial conditions, visualizing the multistability in model (1). For the tree shown in black color, the starting point was chosen at $c = -1$, for which the system has a single fixed point P1(2,0) with coordinates (I, 10 * ($-0.2I + c$)) in correspondence with (6). As the parameter c increases, we see a cascade of period-doubling bifurcations and the development of a chaotic attractor based on this fixed point. Fig. 6a depicts the projection of the variable x_n, whose amplitude does not exceed 25 in the given range of the parameter c. A further increase in the parameter leads to the appearance of high-amplitude overshoots. With red color in Fig. 5a we show the bifurcation tree built with inheritance from the point $c = 0.75$ for $x_0 = 2.64$, $y_0 = 2.22$. For the given parameter values and initial conditions, map (1) reveals one more stable fixed point P3(2,0) coexisting with a period-2 cycle that has arisen on the basis of the point P1. As the parameter c increases chaos also develops via a cascade of period-doubling bifurcations on the basis of the point P3. Fig. 5b shows zoomed fragment of bifurcation trees where the development of chaotic attractors is observed. First, we can observe the coexistence of cycles of different periods for some parameters, and it also is possible to find multistability between different chaotic attractors.

Fig. 5c shows the structure of the basins of attraction of the coexisting chaotic attractor and period-4 cycle for $c = 0.855$. The areas of initial conditions leading to a chaotic attractor are marked with gray color, areas of initial conditions leading to the period-8 cycle is marked with blue color. Attractors are also shown in Fig. 5c, the chaotic one is in black, and the cycle-4 is in red. As can be seen from the figure, the chaotic attractor for the specified values of the parameter is an 8-component chaotic attractor. At the same time, the basin of attraction has a complex fractal structure. A further increase in the parameter c leads to the development of another chaotic attractor, and Fig. 5d shows examples of two chaotic four-component attractors at $c = 0.86$. These attractors have a similar structure, but different scales of phase space, and are characterized by different values of the Lyapunov exponents. For the attractor based on point P1: Λ_1=0.0869, Λ_2= -1.6927, for another attractor based on point P3: $\Lambda_1 = 0.0815$, $\Lambda_2 = -0.4404$. In Fig. 5e one can see the coexistence between 4-component chaos and a complex developed chaotic attractor at $c = 0.865$, for them the Lyapunov exponents are as follows: $\Lambda_1 = 0.094$, $\Lambda_2 = -1.711$ and $\Lambda_1 = 0.2036$, $\Lambda_2 = -0.372$, respectively. A further increase in the parameter c leads to the destruction of the chaotic attractor that arose on the basis of the point P3 as a result of the crisis, and only the chaotic attractor that arose on the basis of the point P1 remains.

When the parameter c decreases from $c = 0.75$ (Fig. 5a), one can see the bifurcation of the birth of an invariant curve, its further development and transformation into a chaotic attractor, and then disappearance as a result of a crisis. The destruction of the attractor corresponds to the saddle-node bifurcation point (l_{SN}, in Fig. 4b), where the fixed points P3 (0,2) and P2(1,1) merge. Next, we consider the features of the chaotic attractor that arose as a result of the destruction of the invariant curve in more detail.

3.2. Destruction of invariant curve

As mentioned above, in the Chialvo map a bifurcation of the invariant curve birth is possible. An invariant curve may lose its smoothness as the parameters change, break down, and, as a result, a chaotic attractor can form. We singled out two regions where the quasi-periodicity and its destruction are observed, when describe main structure of parameter plane (Q_1 and Q_2 in Fig. 4c). Let us consider these

[1] Note, that for an endomorphism significant impact for formation of chaotic attractors brings foldings occurred when attractor cross a line of Jacobian vanishing (4) [33], we discuss it in detail in Section 3.2.

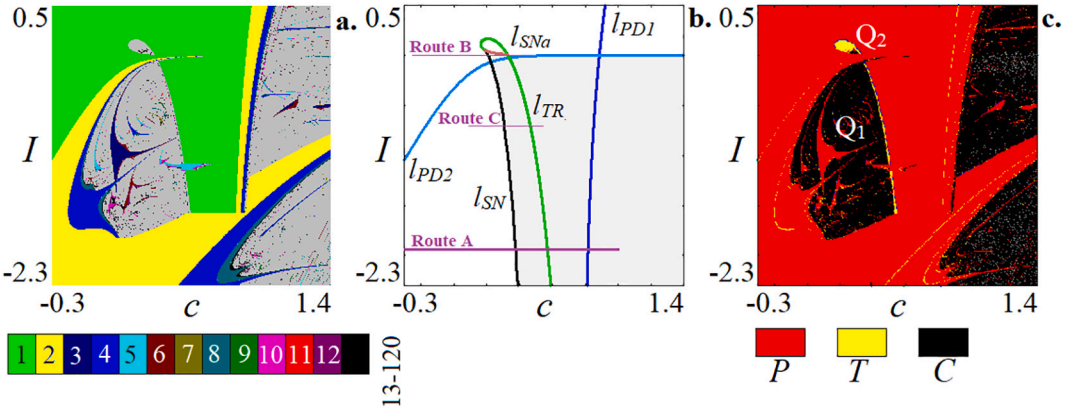

Fig. 4. Parameter plane structure in the area of complex dynamics of Chialvo map (1) at $a = 0.9$, $b = 0.2$. a. The chart of dynamical regimes; b. Two-parametric bifurcation diagram; c. The chart of Lyapunov exponents. l_{PD1}, l_{PD2} are lines of period-doubling bifurcations; l_{SN}, l_{SNa} are lines of saddle-node bifurcations; l_{TR} is line of Neimark-Sacker (invariant curve birth) bifurcation.

Table 1
Accordance of dynamical regimes, signature of Lyapunov's exponents and their designation on the chart of Lyapunov exponents.

Dynamical regime	Label	Signature of the LEs spectrum	Color on the chart
fixed point	*P*	$(0 > \Lambda_1 > \Lambda_2)$	red
invariant curve	*T*	$(\Lambda_1 = 0, 0 > \Lambda_2)$	yellow
chaos	*C*	$(\Lambda_1 > 0, \Lambda_2 < 0)$	black
hyperchaos	*H*	$(\Lambda_1 > 0, \Lambda_2 > 0)$	white

regions in more detail and the chaotic attractors that are observed in them.

In Section 3.1, we could see that on the basis of the fixed point P3 (2,0), as a result of the Neimark-Sacker bifurcation, an invariant curve is born, which then transforms into a chaotic attractor. This scenario occurs with a decrease in the parameter *c* and occupies a small area in the parameter space, since the chaotic attractor disappears simultaneously with the saddle-node bifurcation of the fixed points P2(1,1) and P3(0,2). The area Q_1, where such an invariant curve exists, is a very narrow strip along the torus birth line on the parameter plane. Fig. 6 shows examples of attractors corresponding to the destruction of the invariant curve when the parameter *c* varies for $I = -1.94$. Fig. 6a shows an invariant curve on which 7 bends are formed, in the vicinity of which seven pairs of fixed points appear when entering the synchronization tongue.

Destruction of invariant curves in 2D non-invertable maps may occur in different ways [26,27,33–35]. One of possibility it is the appearance of intersections of the invariant curve with critical line LC_{-1} (where the Jacobian vanishes, see conditions (4)). In Fig. 6 we depict a generating segment of LC_{-1} with red line, which corresponds to the critical line (4), $x = 18/7 \approx 2.57$ and 20 images of the generating segment with blue lines. As we can see in Fig. 6a the (smooth) invariant curve has no intersections with this line and all its images, although these images will approach to the invariant curve that is asymptotically stable. If we decrease parameter *c*, then the invariant curve becomes resonant at $c \approx 0.562$ (two 7-period orbits appear) and at $c \approx 0.5615$ it crosses the critical line LC_{-1}. Fig. 6b presents the example of such resonant invariant curve at $c = 0.561$. Zoomed fragment shows that the images of critical line LC_{-1} can cross the invariant curve. Further, the period-7 orbit undergoes period-doubling bifurcation and chaotic attractor occurs. As it is shown in [33], when LC_{-1} intersects the invariant curve, an annular absorbing area appears bounded (outside and inside) by images of the generating segment LC_{-1}. Example of chaotic attractor and its absorbing area are shown in Fig. 6c for $c = 0.5555$. The attractor is characterized by the following Lyapunov exponents: $\Lambda_1 = 0.03$, $\Lambda_2 = -0.02$.

For positive values of the parameter *I* the picture of bifurcation lines changes, and one can see that another saddle-node bifurcation line (l_{SNa}, in Fig. 4b) appears and the saddle-node bifurcation lines intersect, as well as with the bifurcation line of the birth of an invariant curve (l_{TR} in Fig. 4b). Let us consider the region Q_2 of the parameter space in more detail.

Fig. 7 shows a zoomed fragment of the Lyapunov exponent chart (Fig. 7a) and a two-parameter bifurcation diagram (Fig. 7b). The bifurcation line of the birth of an invariant curve (l_{TR}) appears before the birth of the points P2(1,1), P3(0,2) and has a boundary with the region of a stable fixed point P1(2,0), thus, in the region Q_2, the birth of an invariant curve occurs based on the fixed point P1(2,0). Fig. 7c shows an example of a one-parameter bifurcation diagram for $I = 0.1$. In this case, at $c \approx 0.1645$, the point P1(2,0) undergoes a Neimark-Sacker bifurcation and turns into an unstable focus P1(0,2). With a further increase in the parameter *c*, the reverse Neimark-Sacker bifurcation occurs ($c \approx 0.2854$) and the fixed point P1 again becomes stable. Inside the region bounded on both sides by the Neimark-Sacker bifurcations, one can observe a stable invariant curve and very narrow synchronization tongues.

With decreasing of parameter *I*, two lines of saddle-node bifurcations appear in the bifurcation diagram (Fig. 7b), as a result of which the multistability described in Section 3.1 develops. For $0 < I < 0.05$, a pair of saddle-node bifurcation lines is observed, so a pair of fixed points is born on one boundary and merges on the other. Fig. 7d shows a one-parameter bifurcation diagram corresponding to such bifurcations. At the same time, on the basis of the point P3, with an increase in the parameter *c*, the Neimark-Sacker bifurcation also occurs and the point P3(2,0) becomes an unstable focus P3(0,2), while the point P3 is approximately the same as the point P1.

Inside the Q_2 quasi-periodic region, the development of chaotic behavior is observed. The two-parameter diagrams (Fig. 7a, b) clearly show that chaos is born as a result of the destruction of the invariant curve, while the saddle-node bifurcation lines are located below the chaos region. Thus, the development of chaos occurs in the vicinity of the unstable focus P1(0,2) and other fixed points do not participate in the formation of the attractor.

Fig. 7e and f present examples of chaotic attractors from the region Q_2. Both kinds of attractors have intersection with the non-zero critical line (4) and development of chaos is associated with folding of the invariant curve. Fig. 7f clearly shows the invariant curve, which has just begun to fold and finally break down. With blue lines we depict internal and external boundaries of absorbing domain obtained with iterations of the generating segment of critical line (LC_{-1} in Fig. 7e, f). Such a chaotic attractor is characterized by a small positive Lyapunov exponent: $\Lambda_1 = 0.039$, $\Lambda_2 = -0.1392$. With an increase in the parameter *c*, the development of a chaotic attractor is observed, it becomes more complex (Fig. 7f), while the largest Lyapunov exponent increases, and the second

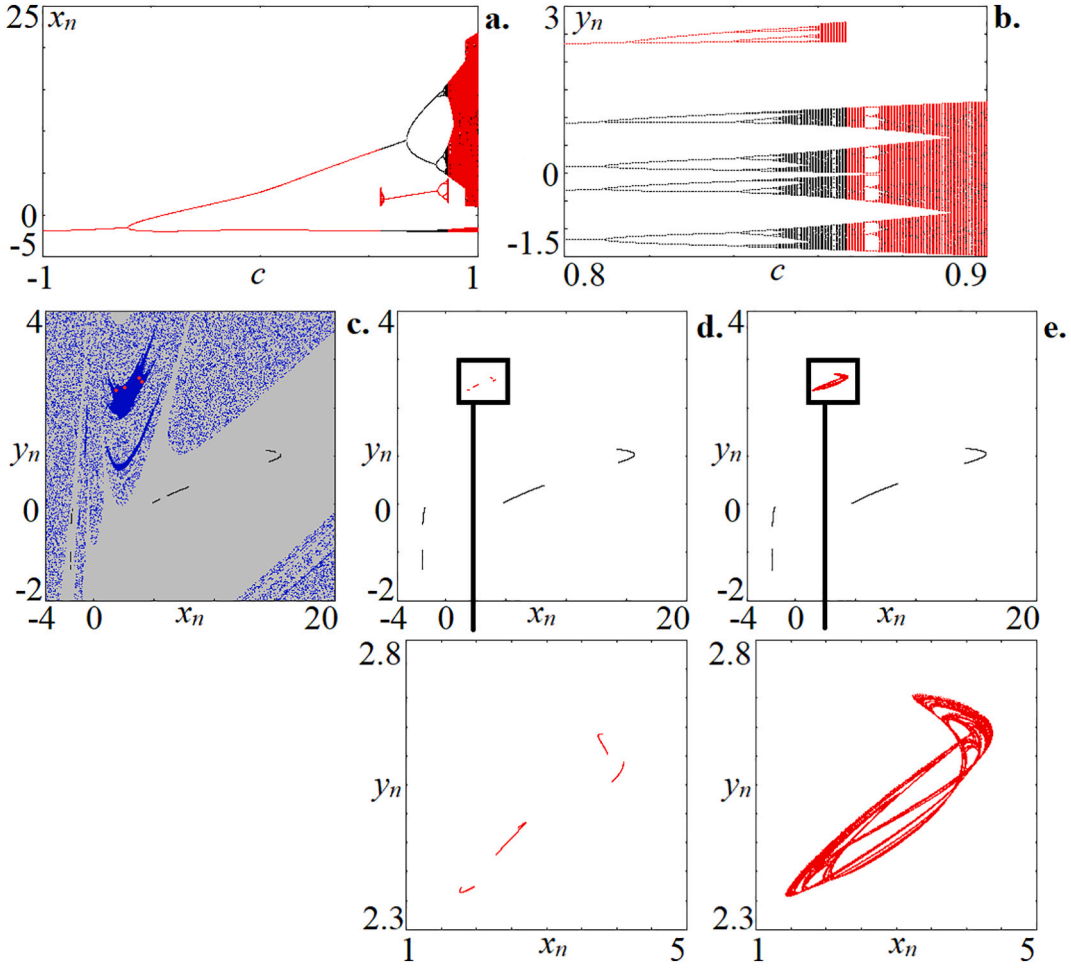

Fig. 5. Chaos occurred via cascade of period-doubling bifurcations and multistability in Chialvo map (1) at $a = 0.9$, $b = 0.2$, $I = -1.94$. a., b. bifurcation trees built for different initial conditions (red and black colors, description in the text); c. coexisting attractors (period-4 cycle and 4-components chaotic attractor) and their basins of attraction, $c = 0.855$; d. coexisting 4-components chaotic attractors, $c = 0.86$; e. coexisting chaotic attractors, $c = 0.865$. (For interpretation of the references to color in this figure legend, the reader is referred to the web version of this article.)

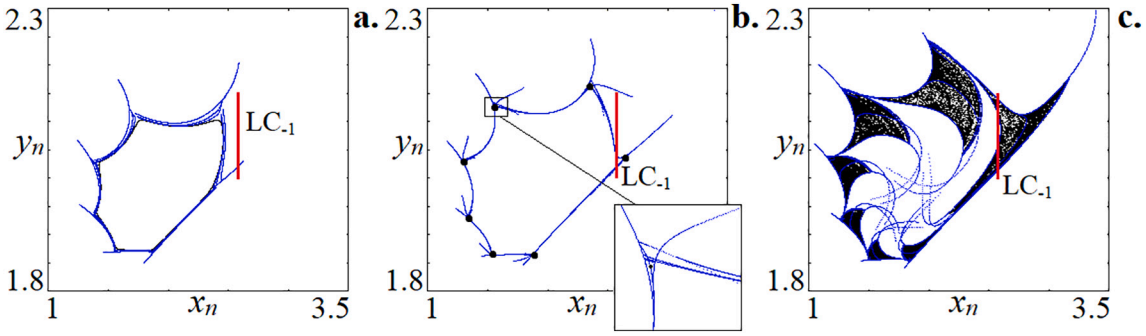

Fig. 6. Destruction of invariant curve in parameter plane area Q_1, $a = 0.9$, $b = 0.2$, $I = -1.94$. a. invariant curve, $c = 0.563$; b. resonant invariant curve, $c = 0.561$; c. chaotic attractor occurred via destruction of invariant curve, $c = 0.5555$.

remains approximately the same as it was: $\Lambda_1 = 0.0543$, $\Lambda_2 = -0.1397$. Further variation of the parameters can lead to the development of chaotic behavior, as well as the formation of a *snap-back repeller*, or as we call it *singular Shilnikov chaotic attractor*. In the following Sections 3.3 and 4, we consider Shilnikov chaotic attractors and their singularities in Chialvo map (1).

3.3. Singular discrete Shilnikov attractor

A universal scenario leading to the emergence of spiral chaos in multidimensional flows, i.e. a strange attractor containing a saddle-focus equilibrium, was proposed by Shilnikov in [21]. This scenario can occur in one-parameter families of flows, and its main stages, as a parameter varies, are as follows (see Fig. 8a): (i) a stable equilibrium; (ii) a stable limit cycle, which appears under a supercritical Andronov-Hopf bifurcation with the equilibrium that becomes a saddle focus with two-

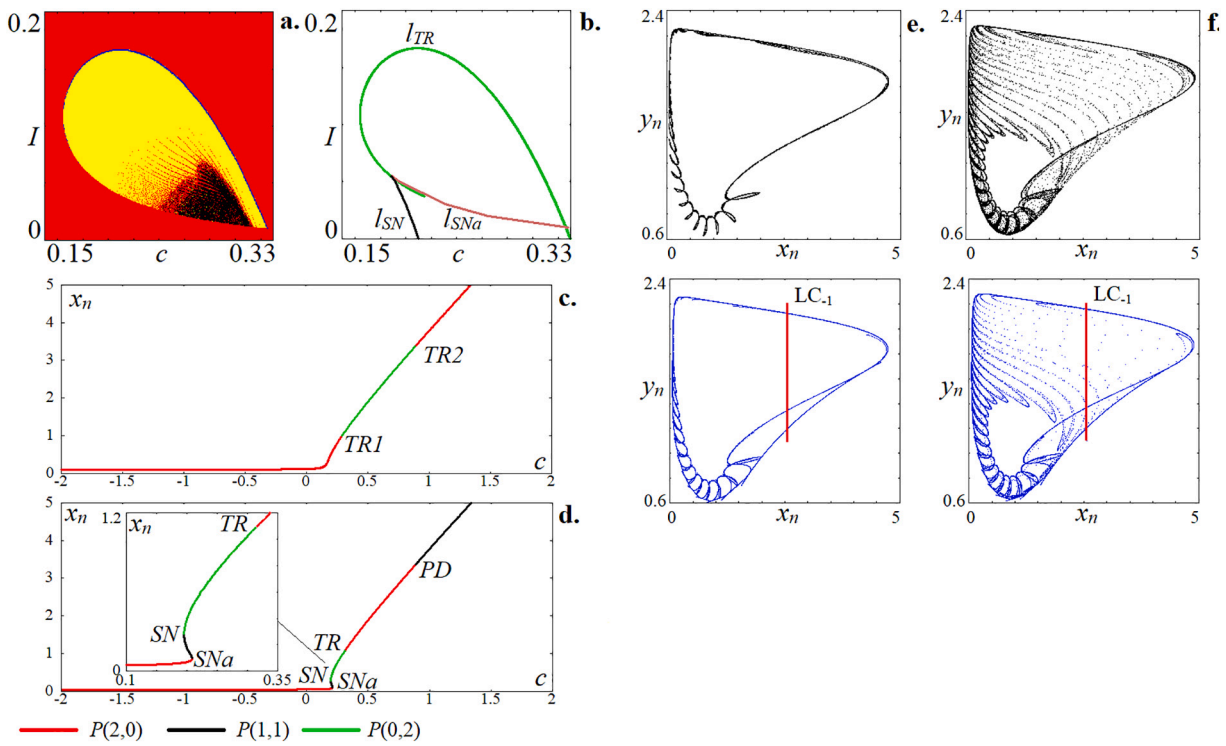

Fig. 7. Destruction of invariant curve in parameter plane area Q2, $a = 0.9$, $b = 0.2$. a. the chart of Lyapunov exponents; b. two-parameter bifurcation diagram: l_{TR} is Neimark-Saker (torus birth) bifurcation line (green), l_{SN}, l_{SNa} are saddle-node bifurcation lines (black, brown, respectively); c. one-parameter bifurcation diagram, $c = 0.1$; d. one-parameter bifurcation diagram, $c = 0.04$; phase portraits and absorbing domain of attractors: e. $c = 0.267$, $I = 0.04$; f. $c = 0.272$, $I = 0.04$. (For interpretation of the references to color in this figure legend, the reader is referred to the web version of this article.)

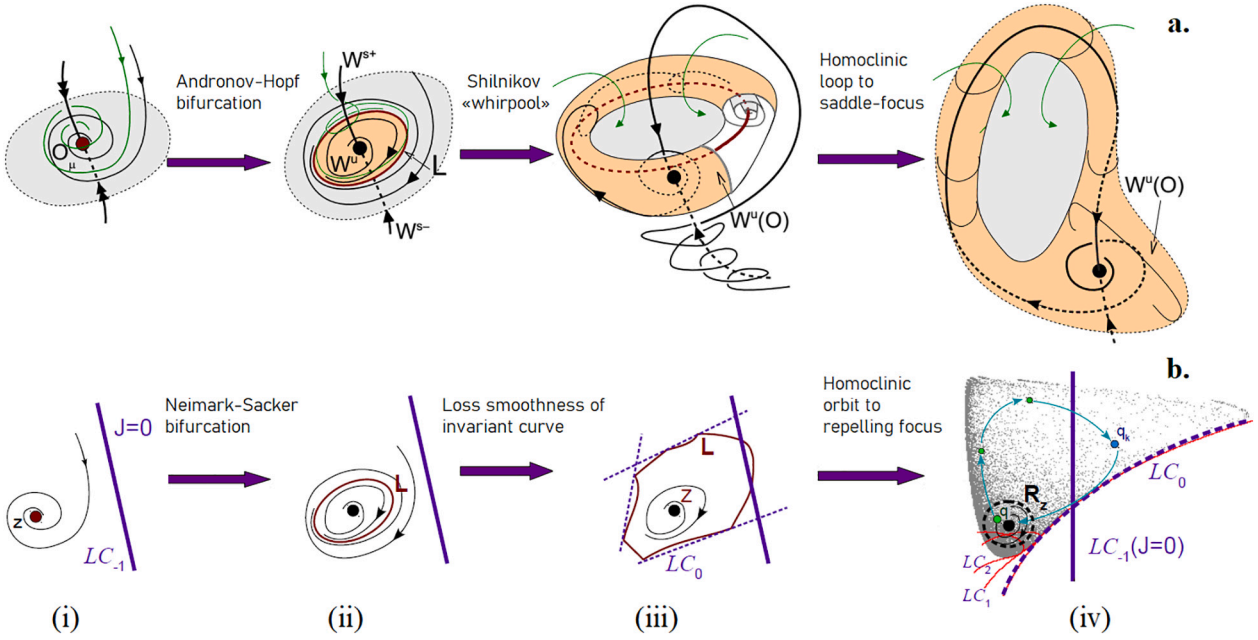

Fig. 8. a. Sketch for scenario of the Shilnikov attractor formation in the case of 3D flow: (i) a stable equilibrium O_μ; (ii) O_μ is the saddle-focus with two-dimensional unstable manifold W^u, attractor is the limit cycle L; (iii) the so-called Shilnikov whirlpool is created, when $W^u(O)$ starts to wind onto the cycle; (iv) the Shilnikov attractor occurs when homoclinic orbits to the saddle-focus equilibrium are created;
b. Sketch for scenario of the Shilnikov singular attractor formation in the case of 2D endomorphism: (i) a stable focus fixed point z; (ii) z is the unstable focus and attractor is the closed invariant curve L; (iii) the invariant curve L crosses critical line where $J = 0$: a kind of "whirlpool" is formed and orbits get an opportunity to jump over L there and back; (iv) the Shilnikov singular attractor occurs when homoclinic orbits to the unstable focus z appear.

dimensional unstable manifold W^u; (iii) the so-called Shilnikov whirlpool is created, when $W^u(O)$ starts to wind onto the cycle (multipliers of the cycle become complex conjugate) and, what is important, all orbits from an absorbing domain are drawn into this "whirlpool"; (iv) the Shilnikov attractor occurs when homoclinic orbits to the saddle-focus equilibrium are created (and the limit cycle and all visible stable invariant subsets from the whirlpool lose stability).

An analogous type of scenario leading to the appearance of discrete Shilnikov attractor for three-dimensional maps was proposed in [22,23,31]. But in this case, the corresponding scenario starts with a stable fixed point and its supercritical Neimark-Sacker bifurcation after which a closed invariant curve is born and the fixed point becomes a saddle-focus with two-dimensional unstable manifold. In multidimensional flow systems, an analogous bifurcation can occur with a stable limit cycle and it is accompanied by the birth of a stable two-dimensional torus (an invariant curve in the Poincaré section).[2]

Remark 1. The discrete Shilnikov attractor was first found in [22,23] in the case of a three-dimensional diffeomorphism of the form

$$\begin{aligned} x_{n+1} &= y_n, \\ y_{n+1} &= z_n, \\ z_{n+1} &= M - Bx_n + Cz_n - y_n^2, \end{aligned} \tag{9}$$

that is a quadratic three-dimensional map with the constant Jacobian $J = B$. For $B = 0$ map (9) becomes probably the most famous two-dimensional endomorphism:

$$y_{n+1} = z_n, \quad z_{n+1} = M + Cz_n - y_n^2. \tag{10}$$

We called it the Mirá map in [43], since it was introduced yet in the paper [44] by C. Mirá and has been studied in great details in the book [33]. Also, map (9) was called 3D Mirá map. Note that the discrete Shilnikov attractors exist in map (9), including for all sufficiently small B [22,23,45]. Then, they will have a topological limit as $B \to 0$, which is the same that we call two-dimensional *singular discrete Shilnikov attractor*.

For two-dimensional maps, a stable invariant curve can appear via a supercritical Neimark-Sacker bifurcation with a stable focus fixed point that becomes unstable focus. Then, this invariant curve can break down and a strange attractor of torus-chaos type can appear. And this can be considered the last stage in the development of chaos in the case when the map T under consideration is a diffeomorphism. However, if T is non-invertable map (endomorphism), then this scenario can be continued till the appearance of a singular Shilnikov attractor. The stages of the corresponding scenario, see Fig. 8b, will be very similar to those in the Shilnikov original scenario, compare Fig. 8a and b. The conspicuous difference is only in partial details: how the invariant curve breaks down and how homoclinics to the unstable saddle-focus appear. In stage (iii) (Fig. 8b) the curve L crosses the line LC_{-1} and folds along the critical line $LC_0 = T(LC_{-1})$. It is a kind of "whirlpool" is formed and orbits get an opportunity to jump over L there and back. In stage (iv) chaos is formed and homoclinic orbits to the unstable focus z appear: a homoclinic orbit has a point q in a repelling domain R_z of z such that $T^{k+1}(q) = z$ for some integer k. This give us a mechanism for instant returning phase orbits to a neighborhood of the unstable focus, which means the existence of a snap-back repeller [25–27]. In this case we say that a *singular Shilnikov attractor is formed when this spiral snap-back repeller is an attractor*.

[2] The discrete Shilnikov attractor can occur when the two-dimensional unstable and one-dimensional stable manifolds of the saddle-focus fixed point begin to intersect [21–23]. Since the appearing attractor contain entirely the two-dimensional unstable manifold of the saddle-focus, it can be hyperchaotic. For flow systems their dimension must be $N \geq 4$, and examples of hyperchaos, when an attractor absorbs a saddle-focus cycle with a two-dimensional unstable manifold, are known, see e.g. [41,42].

Such a situation is also possible in Chialvo map (1). To detect the existence of a homoclinic orbit to the fixed point, the so-called chart of minimal distance was constructed. Fig. 9 shows a fragment of this chart around the region Q_2. The minimum distances from the attractor to the fixed point is calculated according to the following rule:

$$\begin{aligned} \rho_{\min} &= min(\rho_n), \\ \rho_n &= \sqrt{(x_n - x_{EP})^2 + (y_n - y_{EP})^2}, \end{aligned} \tag{11}$$

where x_{EP}, y_{EP} are the coordinates of the fixed point. One-parameter bifurcation diagrams (Figs. 3b, 7d) showed that the unstable focus is the fixed point with the maximum value in variable x_n. When calculating the minimum distance, we find all fixed points, and calculated the distance between attractor and point P1, or point P3 (in the case when three fixed points exist). We marked with black the color on the parameter plane areas where the distance is exactly zero ($\rho_{\min} = 0$), i.e. attractor is the fixed point. Shades of gray mark different values of the minimum distance in accordance with the palette presented in Fig. 9. Points marked in red on the chart, where the minimum distance is in interval: $0 < \rho_{min} \leq 10^{-3}$. Thus, the areas marked in red correspond to points in the parameter space where the unstable fixed point becomes very close to the attractor and, in fact, it may gets homoclinics, which may indicate the formation of a singular chaotic Shilnikov attractor.

Fig. 9b and c show examples of two chaotic attractors from the region Q_2 with small $\rho_{\min}$. It seems that the vicinity of the fixed points is filled densely with phase trajectories for both attractors. However, the enlarged fragments of the vicinity of the unstable focus in Fig. 9d and e show that the first attractor (from Fig. 9b) most likely is not snap-back repeller (Shilnikov attractor). See details below.

Fig. 9b shows a chaotic attractor for $c = 0.27$, $I = 0.027$, which is characterized by the following Lyapunov exponents: $\Lambda_1 = 0.0455$, $\Lambda_2 = -0.2769$. The attractor has a complex structure, one can see thin lines corresponding to the lines of the destroyed invariant curve and phase trajectories in the vicinity of these lines. The red dot in Fig. 9d marks an unstable focus with coordinates (0.86057, 0.97885) and eigenvalues $\lambda_{1,2} = 1.001669 \pm i0.3956$. On the enlarged fragment in the vicinity of the unstable focus, it is clearly seen that the trajectories, despite being very close to the focus, are distant from it, i.e. the focus does not belong to the chaotic attractor. In this case, the minimum distance between the points of the attractor and the unstable focus is: $\rho_{\min} = 4.3 * 10^{-4}$.

Fig. 9c demonstrates an attractor constructed for $c = 0.3$, $I = 0.029$. It is also filled inside with phase trajectories, however, the points are fairly uniformly distributed over the attractor, there is no accumulation of points along the lines, as in Fig. 9b. This attractor is characterized by the following Lyapunov exponents: $\Lambda_1 = 0.0968$, $\Lambda_2 = -0.04$. As can be seen, the largest Lyapunov exponent has more than doubled in comparison with case in Fig. 9b, while the second Lyapunov exponent has decreased in absolute value by almost an order of value. The unstable focus with coordinates (1.0145, 0.9711) and eigenvalues $\lambda_{1,2} = 0.928438 \pm i0.4432$ is inside the chaotic attractor and it is clearly seen that the entire enlarged fragment of the neighborhood of the fixed point is uniformly filled with imaging points (Fig. 9e), which indicates that the unstable focus gets homoclinics and chaotic attractor (of snap-back repeller type) appears. The minimum distance from the attractor to the unstable focus is $\rho_{\min} = 1.2 * 10^{-5}$.

In the region of quasi-periodicity and chaos Q_1 (Fig. 4c), there are also points where the minimal distance between the attractor and the unstable point is close to zero. Fig. 10a shows a chart of minimal distances near region Q_1, where the main bifurcation lines of fixed points are also represented. On the chart, as well as in Fig. 9a, black regions are those where the attractor is a stable fixed point. Note that near the region Q_1, bifurcations occur according to the diagram of Fig. 3b. As a result of the saddle-node bifurcation, a pair of fixed points is born, one of which (P3) becomes an unstable focus in a certain range of parameters. As c increases, the reverse Neimark-Sacker bifurcation occurs and the

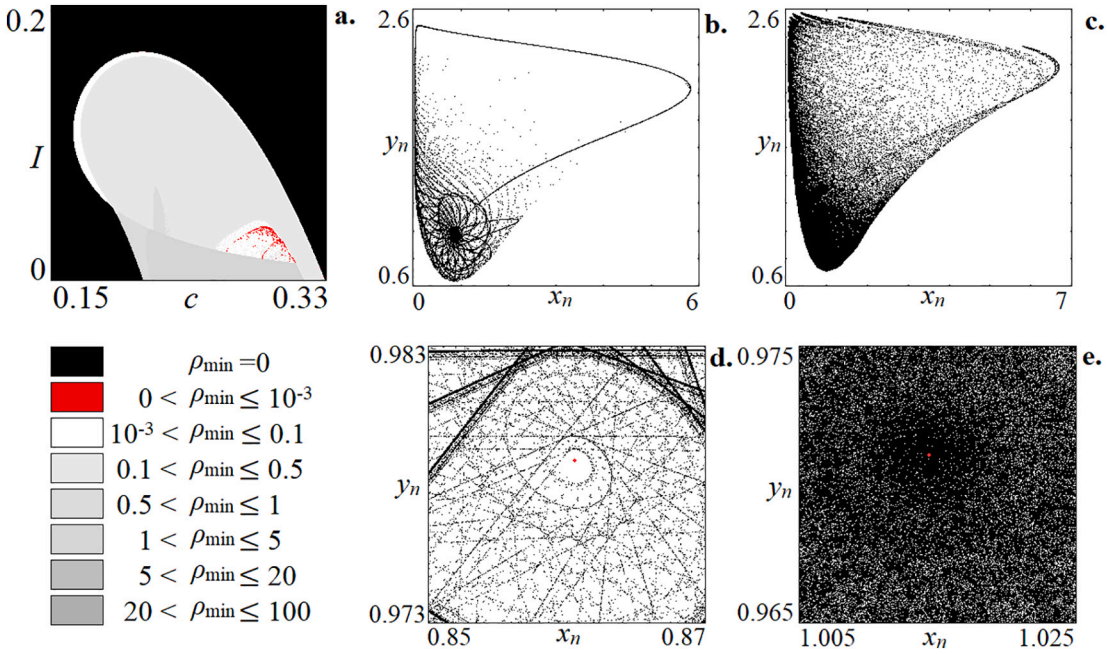

Fig. 9. Illustrations of singular discrete Shilnikov chaotic attractors in area Q_2 of parameter plane (c, I) for Chialvo map (1) with $a = 0.9$, $b = 0.2$. a. the chart of minimal distances between the fixed point P1 and the attractor; phase portraits and their enlarged fragments corresponding to chaotic attractors having a small minimal distance between the attractor and the unstable focus, b. $c = 0.27$, $I = 0.027$; c. $c = 0.3$, $I = 0.029$.

unstable focus becomes stable. This is a soft bifurcation, since when the parameter c decreases accordingly, one can observe the classical supercritical Neimark-Sacker bifurcation, as a result of which a stable invariant curve is born and then it can break down and transform into chaos. For this unstable focus P3 the minimal distance (from an attractor) was calculated. All red areas in Fig. 10a (where the minimal distance is close to zero) are obtained to be located to the right of the saddle-node bifurcation line, therefore, it is precisely the case when the unstable focus can get homoclinics. Thus, we can assume the formation of a singular discrete chaotic Shilnikov attractor.

Fig. 10b-10e show examples of chaotic attractors on various scales with decreasing parameter c and a fixed parameter $I = -0.69$ (purple line in Fig. 10a), the position of the unstable focus P3(0,2) is marked with red dots. Table 2 presents the main characteristics of attractors for those presented in Fig. 10b-10e examples: coordinates of the fixed point, eigenvalues, Lyapunov exponents, minimal distance $\rho_{\min}$.

Fig. 10b shows a chaotic attractor (torus-chaos) that is not certainly a snap-back repeller. The unstable focus P3 is well-distanced from the attractor, which can be seen visually and is also confirmed by the calculated value of $\rho_{\min}$ for long time series. For phase portraits in Fig. 10, for each fragment, $2 * 10^5$ points were built, while for fragments, the length of the time series itself could be up to 10^9 iterations (in Table 2, we indicated $N_{iter}^{\max}$ is specific number of iterations for which $2 * 10^5$ points were placed in the minimal fragment). In the chart of minimal distance, a gray band is clearly visible at the border of the Neimark-Sacker bifurcation line (l_{TR}), which just corresponds to the invariant curve and chaotic attractors, distant from the fixed point (unstable focus). Such a chaotic attractor is characterized by positive and negative Lyapunov exponents, which are quite close to each other in absolute value.

With a decrease in the parameter c, red areas appear on the chart of minimal distances, the corresponding attractor is shown in Fig. 10c at $c = 0.451$. The full-scale phase portrait allows us to conclude that the phase trajectories come very close to the unstable focus. For a more accurate analysis, enlarged fragments of the attractor were built; they are shown below in Fig. 10c, which clearly shows that a very small neighborhood of the unstable focus remains unfilled. Both Lyapunov exponents for such an attractor increase, while the positive exponent becomes more than twice as large as the second exponent in absolute value.

Further decrease in the parameter c leads to the appearance of homoclinics to the unstable focus after the attractor intersects also the second critical line ($x = 0$), and an expansion of the chaotic attractor is observed, see Fig.10e, 10f.[3] The enlarged fragments of the attractors show that the points fill the vicinity of the unstable focus. The points also visit other regions of the phase space. The minimal distance from the attractor to the unstable focus becomes about 10^{-5}. At the same time, Lyapunov exponents continue to grow.

Thus, our numerical simulations show that in both regions Q_1 and Q_2 where invariant curves break down, snap-back repellers can occur. By the Marroto definition [25,32] a snap-back repeller is an invariant set having a repelling fixed (periodic) point and a nondegenerate homoclinic orbit to it. The Chialvo map (1) has the complex form and therefore we can not obtain analytical expressions even for coordinates of its fixed points that makes a possibility for analytical proofs almost unrealistic. But we can check existence of homoclinic trajectories numerically with high accuracy. One of the homoclinic point (x_{pr}, y_{pr}) should be the preimage of the unstable focus (x_{EP}, y_{EP}), i.e. the following relation take place

$$x_{EP} = x_{pr}^2 exp\left[\frac{y_{EP} - c}{a} + \frac{b - a}{a} x_{pr}\right] + I,$$
$$y_{pr} = \frac{y_{EP} - b x_{pr} - c}{a}, \tag{12}$$

Note, that Eq. (12) for considered values of parameters, give three roots. One of them corresponds to the fixed point (x_{EP}, y_{EP}). Two other roots (x_1, y_1) and (x_2, y_2) are such $x_1 < 0$ and $x_2 > 0$. Thus, the root with $x_1 < 0$ is evidently not homoclinic for $I > 0$. The root with $x_2 > 0$ can be

[3] Note, that, even before the snap-back repeller appears, chaotic attractor is surrounded by homoclinic orbits. A contact between external boundary of the invariant area with an invariant set existing outside leads to expansion of attractor, then we obtain the so-called mixed absorbing area and mixed chaotic area [33].

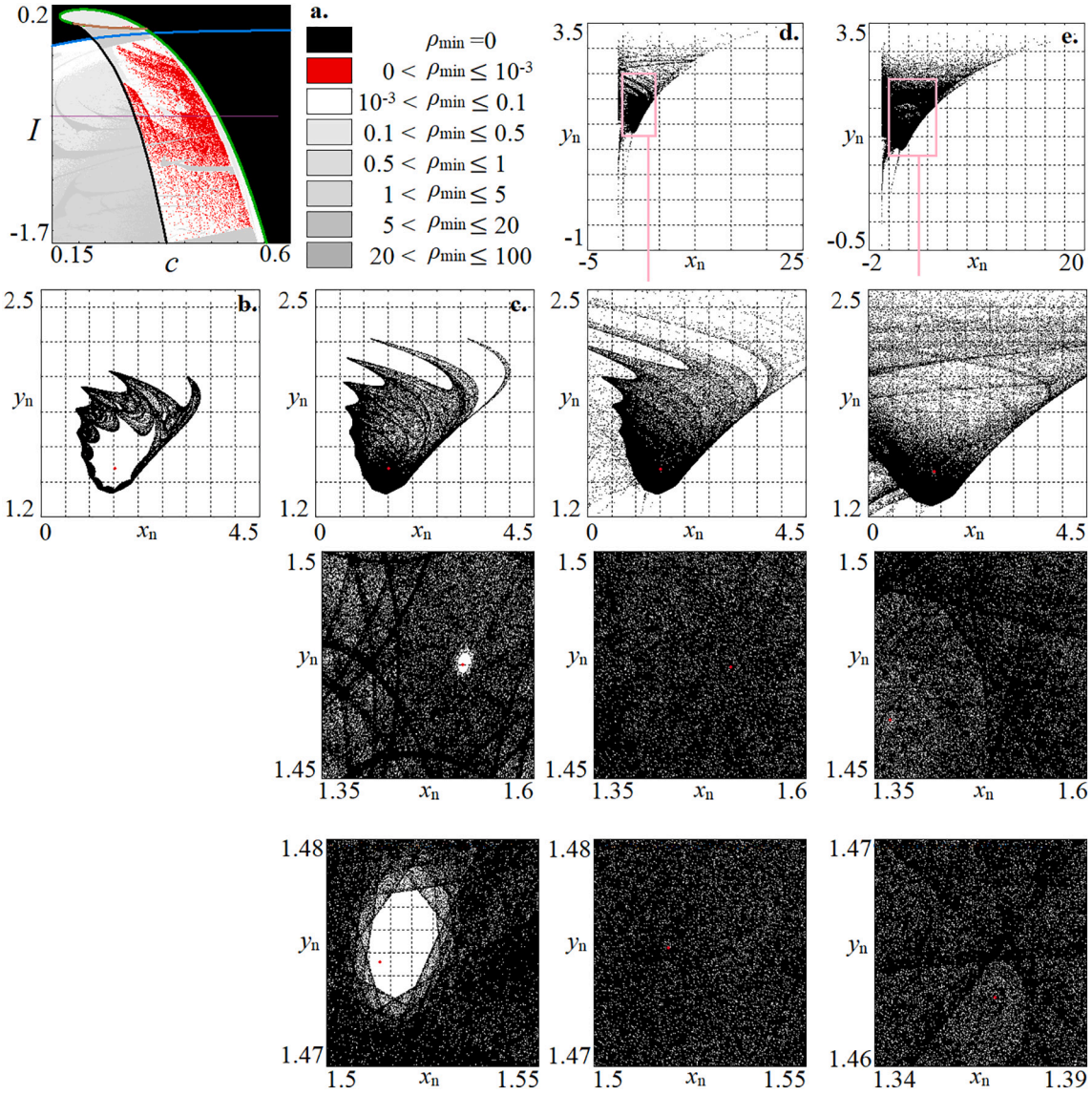

Fig. 10. Illustrations of singular discrete Shilnikov chaotic attractors in area Q_2 of parameter plane (c, I) for Chialvo map (1) with $a = 0.9$, $b = 0.2$. a. the chart of minimal distances between the fixed point P3 and the attractor; phase portraits and their enlarged fragments corresponding to chaotic attractors, $I = -0.69$, b. $c = 0.452$; c. $c = 0.451$; d. $c = 0.45$; e. $c = 0.42$.

Table 2
Characteristics of chaotic attractors presented in Fig. 10.

Parameter c	Fixed points, (x_{EP}, y_{EP})	Eigenvalues, λ_1, λ_2	Lyapunov exponents, Λ_1, Λ_2	Minimal distance, ρ_{min}	Number of iterations, N_{iter}^{max}
0.452	(1.5221, 1.4759)	0.79665 ± i0.657313	0.0612, −0.0535	$1.14 * 10^{-1}$	$2 * 10^5$
0.451	(1.5174, 1.4752)	0.80039 ± i0.657177	0.0956, −0.0482	$2.1 * 10^{-3}$	$4.52 * 10^8$
0.45	(1.5127, 1.4746)	0.80414 ± i0.657022	0.1658, −0.0335	$5.9 * 10^{-5}$	$4.8 * 10^8$
0.42	(1.3685, 1.463)	0.92437 ± i0.641407	0.4421, −0.0966	$1.8 * 10^{-5}$	$1.13 * 10^9$

homoclinic in both cases $I \le 0$ and $I > 0$, therefore we will consider as the preimage namely the root (x_2, y_2). In Fig. 11 we presented iteration diagrams starting with the obtained preimage points (x_{pr}, y_{pr}). As we can see such point goes, theoretically, exactly to the unstable focus (x_{EP}, y_{EP}) but, numerically, its trajectory makes many iterations escaping it. Note that preimage points can be found and for the cases when attractor is not snap-back repeller, in this case preimage points will be localized outside of chaotic attractor.

Such experiment we conduct with trajectories and calculated number of direct jumps to the repelling focus with the accuracy 10^{-4}. During $1.5 * 10^9$ iterations such jumps are happened <20 times for all the mentioned snap-back repellers, and such jumps were not found for those cases where we assume the absence of snap-back repellers.

Thus, we have demonstrated two types of singular discrete chaotic Shilnikov attractors: the first one (Fig. 9c) is localized in the vicinity of the base invariant curve (region Q_1) and this attractor intersect only one non-zero critical curve from (4), namely $x \approx 2.57$; the second attractor (Fig. 10d, e) is bigger then the first one (due to intersection with the both critical lines $x \approx 2.57$ and $x = 0$) and it is observed in region Q_2.

In Section 4 below we consider in more detail main features of the time series corresponding to the appearance of a singular discrete chaotic Shilnikov.

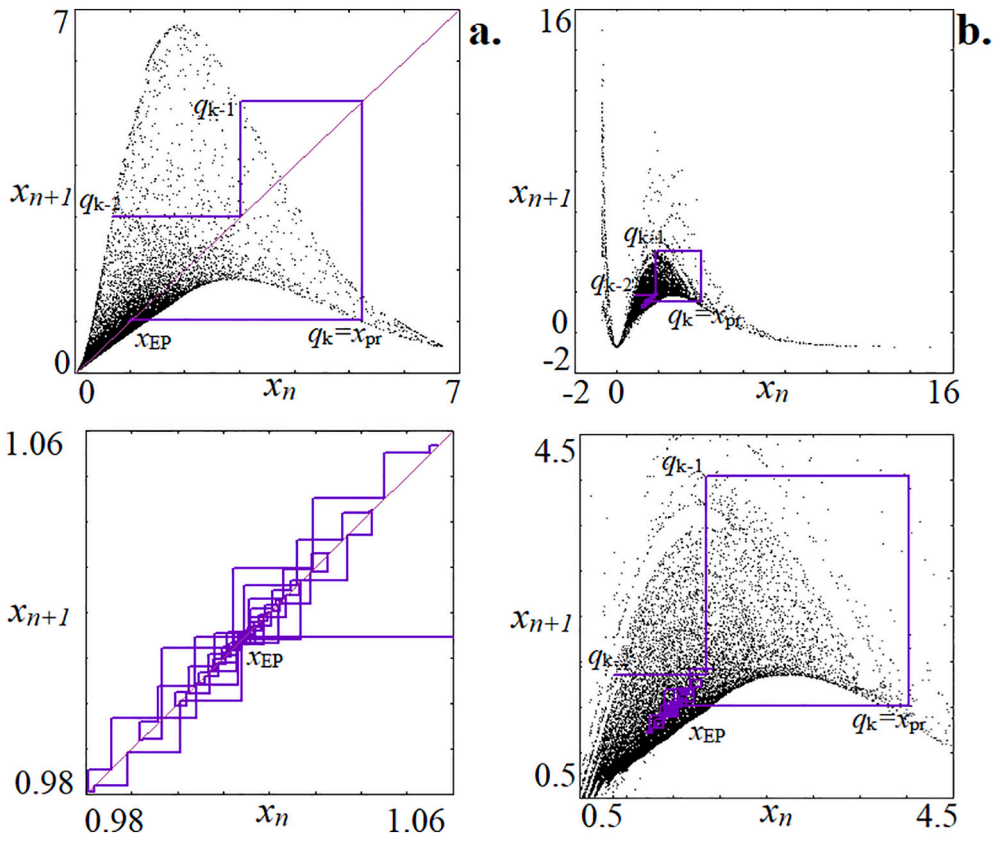

Fig. 11. Iteration diagrams starting from the preimage points (x_{pr}, y_{pr}) of (12) and corresponding attractors. a. $I = 0.029$, $c = 0.3$; b. $I = -0.69$, $c = 0.45$.

4. Time series features of singular discrete chaotic Shilnikov attractors

As mentioned above, singular chaotic Shilnikov attractors are associated with the appearance of homoclinics to an unstable focus. In time series for such attractors, characteristic patterns can be distinguished that correspond to rotating movements of a phase trajectory from a vicinity of the unstable focus. In [36], the features of time series were discussed during the formation of the Shilnikov attractor in the Rosenzweig–MacArthur model which is the flow dynamical system. Despite of Chialvo map (1) is not a flow at all, it is an endomorphism, one can find something similar, but with own peculiarities, on time series associated with the singular Shilnikov attractor.

Fig. 12 presents several typical examples for different areas of the parameter plane (c, I). With black color we depict time series for the attractor with length of 5000 iterations, and with blue color we show enough short transient process for the same values of parameters. Fig. 12b, d, f demonstrate examples of trajectories calculated for initial conditions close to the unstable focus (blue color). Using the bisection method, a fixed point calculated with an accuracy of 10^{-4} was used as the starting point for iteration. All trajectories in Fig. 12b, d, f correspond to Shilnikov singular attractor and have their own peculiarities. Fig. 12b demonstrates the case of the Shilnikov attractor for the region Q_1 at $c = 0.3$, $I = 0.029$ (Fig. 9c). Fig. 12d and f are examples from region Q_2 (Fig. 10d, e). The first example corresponds to the case when the unstable focus is close to chaotic attractor, but homoclinic bifurcation did not happend yet. The attractor in Fig. 12f corresponds to the case when a homoclinic orbit to the unstable focus appears, and also the attractor intersects the second line ($x = 0$) where Jacobian is vanishing. Figures clearly show that the trajectory in the vicinity of the unstable focus performs rotational oscillations around it. A smooth increase in the amplitude occurs up to a certain threshold, and then the trajectory passes through the rest of the attractor. The intervals with rotating are different from the main part of the time series. Depending on the parameters, the duration of the rotation is changed. It is clearly seen, that for the attractor localized near the original invariant curve and having intersection with only one critical line ($x \approx 2.57$), see. Fig. 12b, the rotation takes the longest time, the amplitude increases slowly. When homoclinics did not yet appear but the unstable focus is close to the chaotic attractor (Fig. 12d), the rotations occur to be faster and, when reached the attractor, trajectories no longer approaches very close to the unstable focus. In the case when homoclinics to the unstable focus occur and the attractor intersects both lines of Jacobian vanishing (Fig. 12f), the buildup occurs most rapidly and the region of characteristic rotation in the vicinity of the unstable focus is very small.

If homoclinic orbit to the unstable focus occurs, or even trajectories are very close to it, such intervals will occur in time series and may represent patterns of a special oscillatory activity of a neuron model. To analyze such patterns, one can use various characteristics calculated from long time series.

Fig. 12a-f show examples of short time series (5000 iterations) of Chialvo model (1) for various parameter values, some of which correspond to Shilnikov singular attractors (Fig. 12b, d, f). Table 3 presents the characteristics of the patterns corresponding to the movement of the trajectory in the vicinity of the unstable focus, below we present a description of the characteristics.

Fig. 12a-d present time series for attractors from the region Q_2 of parameter plane (c, I), which were discussed and illustrated in Fig. 11. Time realizations clearly show intervals when the phase trajectory enters the vicinity of the unstable focus and makes several rotations. For Fig. 12a, the minimal distance from the attractor to the unstable focus is 0.114; in this case, we can clearly see that the attractor is distant from the unstable focus. On the time series, patterns similar to blue lines in Fig. 12b, d, e are not observed. For all other examples, the distance from the chaotic attractor to the unstable focus is very small. And in almost every time series, we can identify patterns of atypical activity that

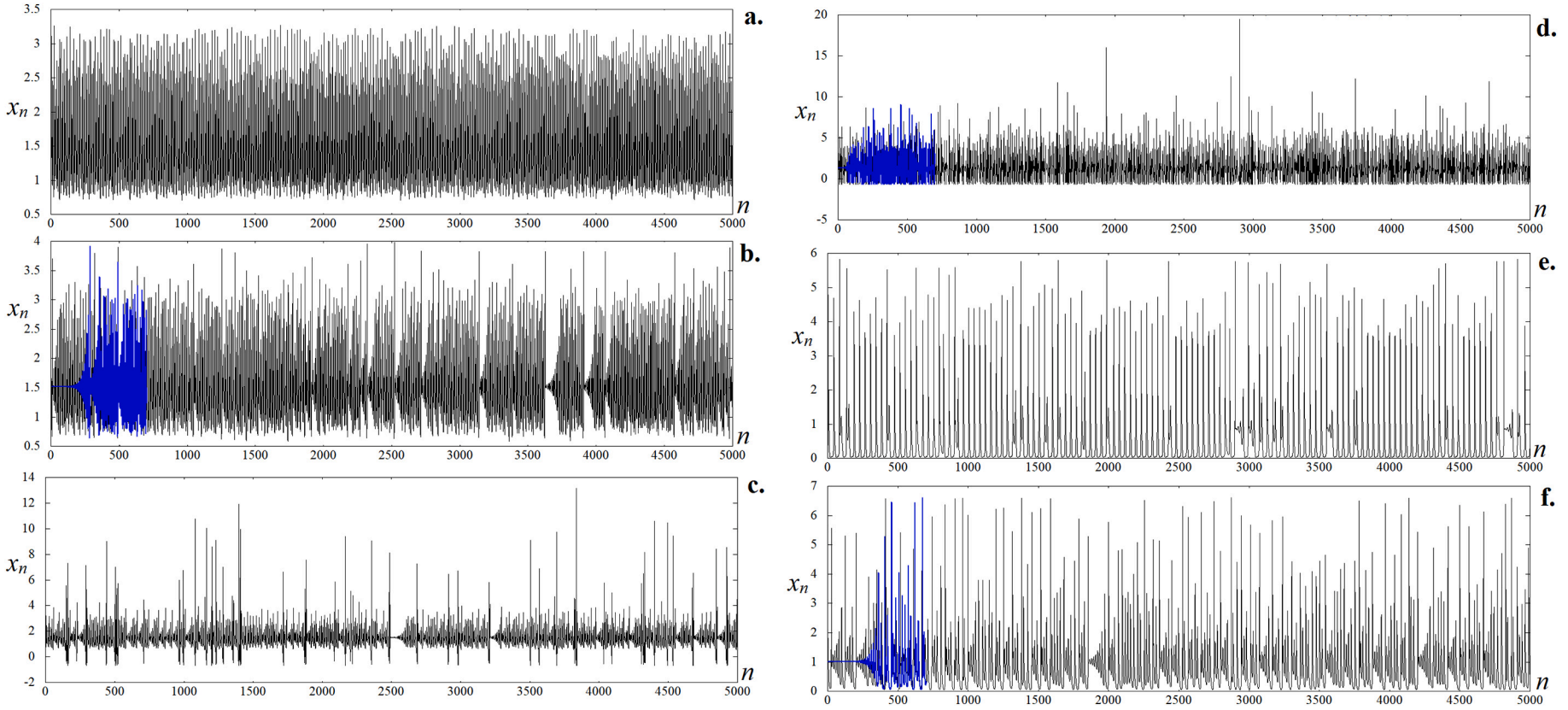

Fig. 12. Time series of Chialvo map (1), demonstrating the appearance of patterns of atypical oscillatory activity associated with the appearance of homoclinics to an unstable focus, $a = 0.9$, $b = 0.2$. a. $c = 0.452$, $I =$ -0.69; b. $c = 0.451$, $I =$ -0.69; c. $c = 0.45$, $I =$ -0.69; d. $c = 0.42$, $I =$ -0.69; e. $c = 0.27$, $I = 0.027$; f. $c = 0.3$, $I = 0.029$. Blue lines demonstrate transient process of the phase trajectories in a small vicinity (10^{-4}) of unstable focuses. (For interpretation of the references to color in this figure legend, the reader is referred to the web version of this article.)

Table 3
Characteristics of patterns arising on time series when an unstable focus is absorbed by a chaotic attractor for Chialvo model (1) for $a = 0.9$, $b = 0.2$.

Parameters	Number of trappings in the vicinity of the unstable focus for a trajectory of length $3 * 10^6$, N_{trap}	Duration of the rotating movements of the phase trajectory from the vicinity of the unstable focus, (average, maximum) τ_{trap}^{aver}, τ_{trap}^{max}	Number of trappings with duration >40 N_{trap}^{40}	Minimal distance, ρ_{min}
$c = 0.452$, $I = -0.69$	0	0	0	$1.14 * 10^{-1}$
$c = 0.451$, $I = -0.69$	107,345	34.58, 119	3745	$2.25 * 10^{-3}$
$c = 0.45$, $I = -0.69$	94,052	20.65, 167	1900	$2.9 * 10^{-4}$
$c = 0.42$, $I = -0.69$	51,106	9.73, 51	11	$7.8 * 10^{-4}$
$c = 0.27$, $I = 0.027$	56,472	23.4, 79	774	$2.16 * 10^{-3}$
$c = 0.3$, $I = 0.029$	86,643	58.17265	3670	$1.3 * 10^{-4}$

correspond to the hit of the phase trajectory in the vicinity of an unstable focus. Such patterns can be classified as a special type of neuron activity that violates the general structure of time series.

For such patterns, dynamical characteristics can be suggested. Table 3 presents these characteristics for long time series ($3 * 10^6$ iterations). Let us describe these characteristic:

- N_{trap} is the number of hits of the trajectory in the vicinity of the unstable focus. To calculate the characteristic, we counted the number of hits in the vicinity of the unstable focus. For the vicinity we took $\delta = 10^{-1}$. Such a characteristic will show the frequency of occurrence of patterns in the time series;
- τ_{trap}^{aver} is the average duration of the trajectory unwinding from the vicinity of the unstable focus. In a numerical experiment, for each hit of the trajectory in the vicinity of the unstable focus, the duration of its stay in the neighborhood was calculated, it was assumed that the rotating movements continue until the moment when the trajectory goes beyond the vicinity with a radius: $\delta = 5 * 10^{-1}$. The maximum value (τ_{trap}^{max}) was obtained, averaged over all $N_{trap}(\tau_{trap})$. Such a characteristic describes the rate of rotating movements of phase trajectory in the vicinity of an unstable focus and, accordingly, the duration of patterns in time series;
- N_{trap}^{40} the number of hits of trajectories in the vicinity of the unstable focus, the duration of rotations of which is 40 or more iterations. This characteristic shows the presence of long-term patterns of atypical oscillatory activity.

The proposed characteristics make it possible to identify time series in which activity patterns are most clearly expressed. This can be determined by the maximum duration of the rotating movements of a phase trajectory. Fig. 12 clearly demonstrates that long-term patterns are the most clearly visible in the case when the homoclinic orbit to unstable focus occurs. The trajectory quite often gets close to unstable focus, which leads to the appearance of long-term patterns, and as a result, the number of hits with duration of >40 is much greater than for attractors in which the unstable focus is distant from the attractor. Also, for this type of attractors, the indicator of the average duration of patterns becomes noticeably longer. Proposed characteristics make it possible to distinguish the case when the homoclinc orbit occurs, while no atypical patterns are observed on the time series. Such an example is shown in Fig. 12d. The distance between the chaotic attractor and the unstable focus is very small, and it is clearly seen in the phase portraits that the trajectories visit the neighborhood of the unstable focus, while the average duration of rotating movements is 8 iterations, the trajectory very quickly runs away from the vicinity of unstable focus, so we do not see patterns of atypical oscillatory activity in time series.

5. Conclusions

We conduct a detailed analysis of dynamics of the Chialvo map (1), which is the simplest model of neuron dynamics in the form of a map. In the parameter space, regions are localized where high-amplitude pulses are observed. The main scenarios of the formation of chaotic orbit behavior are illustrated. These includes the standard scenaria such as those via cascades of period-doubling bifurcations and via break down of closed invariant curves, as well as a new for endomorphisms scenario of emergence of two-dimensional singular Shilnikov attractor is proposed and its numerical implementations are demonstrated.

Note that the formation of Shilnikov singular attractor influence to a character of observed time series: here patterns of atypical oscillatory activity may appear between alternating segments with rotating movements of the phase trajectories near unstable foci. An estimation of the dynamical characteristics of such patterns is carried out for time series of various lengths. It is shown that the appearance of the Shilnikov attractor does not always lead to the formation of clearly visible patterns of atypical oscillatory activity. However, such patterns are well expressed in the case when the strange attractor is a torus-chaos on a threshold of formation of the Shilnikov attractor. At the moment when the latter is formed, the patterns of atypical activity become the most distinct. However, these patterns become very short and indistinguishable in time series when the attractor is expanding due to intersection of both critical lines of Jacobian vanishing (such attractors characterizes by larger the maximal Lyapunov exponent). We propose dynamical characteristics that allow classifying the attractors described above.

The appearance of such patterns of atypical oscillatory activity leads to the destruction of the homogeneity of time series and the formation of features that can be diagnosed for experimental data obtained as a result of EEG, for instance. The described type of atypical oscillatory activity of a neuron model can be used for the study of pathological states of a neuron.

CRediT authorship contribution statement

N.V. Stankevich: Conceptualization, Methodology, Formal analysis, Investigation, Software. **A.S. Gonchenko:** Investigation, Validation, Software. **E.S. Popova:** Validation, Investigation. **S.V. Gonchenko:** Conceptualization, Formal analysis.

Declaration of competing interest

Authors declare that they have no conflict of interest.

Data availability

Data supporting numerical experiments presented in this paper are available from the corresponding author upon reasonable request.

Acknowledgments

The work was carried out with the financial support of the Russian Science Foundation, grant No. 20-71-10048 (Sections 1, 2, 3.1, 3.2, 4, 5). Description of scenario of Shilnikov attractor development was carried out with the financial support of the Russian Science Foundation, grant No. 19-11-00280 (Section 3.3). S. Gonchenko thanks the Theoretical Physics and Mathematics Advancement Foundation "BASIS", Grant No. 20-7-1-36-5, for support of scientific investigations of his group.

Authors thank Laura Gardini and Irina Sushko for fruitful discussion

of this problem. The author also thanks anonymous reviewers for their careful reading and valuable comments.

References

[1] Abarbanel HD, Rabinovich MI. Neurodynamics: nonlinear dynamics and neurobiology. Curr Opin Neurobiol 2001;11(4):423–30.
[2] Izhikevich EM. Dynamical systems in neuroscience. MIT press; 2007.
[3] Marsland S. Machine learning: an algorithmic perspective. Chapman and Hall/CRC; 2011.
[4] McKenna TM, Davis JL, Zornetzer SF, editors. Single neuron computation. Academic Press; 2014.
[5] Hodgkin AL, Huxley AF. Currents carried by sodium and potassium ions through the membrane of the giant axon of Loligo. J Physiol 1952;116(4):449.
[6] Hodgkin AL, Huxley AF. A quantitative description of membrane current and its application to conduction and excitation in nerve. J Physiol 1952;117(4):500.
[7] Hindmarsh JL, Rose RM. A model of neuronal bursting using three coupled first order differential equations. Proc R Soc B Biol Sci 1984;221(1222):87–102.
[8] Shilnikov A, Kolomiets M. Methods of the qualitative theory for the Hindmarsh–Rose model: a case study–a tutorial. Int J Bifurcation Chaos 2008;18(08):2141–68.
[9] Sherman A, Rinzel J, Keizer J. Emergence of organized bursting in clusters of pancreatic beta-cells by channel sharing. Biophys J 1988;54(3):411–25.
[10] Mosekilde E, Lading B, Yanchuk S, Maistrenko Y. Bifurcation structure of a model of bursting pancreatic cells. BioSystems 2001;63(1):3–13.
[11] Cymbalyuk G, Shilnikov A. Coexistence of tonic spiking oscillations in a leech neuron model. J Comput Neurosci 2005;18:255–63.
[12] Shil'nikov AL, Cymbalyuk G. Homoclinic bifurcations of periodic orbits en a route from tonic spiking to bursting in neuron models. Regular Chaotic Dyn 2004;9(3):281–97.
[13] Izhikevich EM, Hoppensteadt F. Classification of bursting mappings. Int J Bifurcation Chaos 2004;11(14):3847.
[14] Ibarz B, Casado JM, Sanjuán MAF. Map-based models in neuronal dynamics. Phys Rep 2011;1-2(501):1–74.
[15] Girardi-Schappo M, Tragtenberg MHR, Kinouchi O. A brief history of excitable map-based neurons and neural networks. J Neurosci Methods 2013;2(220):116–30.
[16] Chialvo DR. Generic excitable dynamics on a two-dimensional map. Chaos, Solitons Fractals 1995;3-4(5):461–79.
[17] Shilnikov AL, Rulkov NF. Subthreshold oscillations in a map-based neuron model. Phys Lett A 2004;2-3(328):177–84.
[18] Wang F, Cao H. Mode locking and quasiperiodicity in a discrete-time Chialvo neuron model. Commun Nonlinear Sci Numer Simul 2018;56:481–9.
[19] Yang Y, et al. Complex dynamic behaviors in a discrete Chialvo neuron model induced by switching mechanism. Cham: International Symposium on Neural Networks. Springer; 2020. p. 61–73.
[20] Bashkirtseva I, Ryashko L, Seoane JM, Sanjuán MA. Noise-induced complex dynamics and synchronization in the map-based Chialvo neuron model. Commun Nonlinear Sci Numer Simul 2023;116:106867.
[21] Shilnikov LP. Bifurcation theory and turbulence. In: Shilnikov LP, editor. Proceedings "Methods in quality theory of differential equations" 1986: 150–165 (in Russia). The theory of bifurcations and turbulence I. Selecta Mathematica Sovetica, 1(10); 1991. p. 43–53 [Translation].
[22] Gonchenko AS, Gonchenko SV, Shilnikov LP. Towards scenarios of chaos appearance in three-dimensional maps. Rus J Nonlin Dyn 2012;1(8):3–28 [Russian].
[23] Gonchenko A, Gonchenko S, Kazakov A, Turaev D. Simple scenarios of onset of chaos in three-dimensional maps. Int J Bifurcation Chaos 2014;24(08):1440005.
[24] Shilnikov LP. A case of the existence of a denumerable set of periodic motions. Dokl Akad Nauk 1965;3(160):558–61.
[25] Marotto FR. Snap-back repellers imply chaos in R^n. J Math Anal Appl 1978;63(1):199–223.
[26] Gardini L. Homoclinic bifurcations in n-dimensional endomorphisms, due to expanding periodic points. Nonlinear Anal Theor Methods Appl 1994;23(8):1039–89.
[27] Gardini L, Tramontana F. Snap-back repellers in non-smooth functions. Regular Chaotic Dyn 2010;15(2–3):237–45.
[28] Rössler OE. An equation for continuous chaos. Phys Lett A 1976;57(5):397–8.
[29] Malykh S, Bakhanova Y, Kazakov A, Pusuluri K, Shilnikov A. Homoclinic chaos in the Rössler model. Chaos 2020;30(11):113126.
[30] Gaspard P, Nicolis G. What can we learn from homoclinic orbits in chaotic dynamics? J Stat Phys 1983;31(3):499–518.
[31] Gonchenko AS, Gonchenko SV. Variety of strange pseudohyperbolic attractors in three-dimensional generalized Hénon maps. Phys D Nonlinear Phenom 2016;337:43–57.
[32] Marotto FR. On redefining a snap-back repeller. Chaos, Solitons Fractals 2005;25(1):25–8.
[33] Mira C, Gardini L, Barugola A, Cathala J-C. Chaotic dynamics in two-dimensional noninvertible mapsvol. 20. World Scientific; 1996.
[34] Frouzakis CE, Gardini L, Kevrekidis IG, Millerioux G, Mira C. On some properties of invariant sets of two-dimensional noninvertible maps. Int J Bifurcation Chaos 1997;7(06):1167–94.
[35] Gardini L, Sushko I, Avrutin V, Schanz M. Critical homoclinic orbits lead to snap-back repellers. Chaos, Solitons Fractals 2011;44(6):433–49.
[36] Bakhanova YV, Kazakov AO, Korotkov AG, Levanova TA, Osipov GV. Spiral attractors as the root of a new type of "bursting activity" in the Rosenzweig–MacArthur model. Eur Phys J Special Top 2018;227(7):959–70.
[37] Ermentrout B. Simulating, analyzing, and animating dynamical systems: a guide to XPPAUT for researchers and students. Philadelphia: SIAM; 2002.
[38] Chowdhury SN, Ray A, Dana SK, Ghosh D. Extreme events in dynamical systems and random walkers: a review. Phys Rep 2022;966:1–52.
[39] Mishra A, Leo Kingston S, Hens C, Kapitaniak T, Feudel U, Dana SK. Routes to extreme events in dynamical systems: dynamical and statistical characteristics. Chaos 2020;30(6):063114.
[40] Ray A, Rakshit S, Ghosh D, Dana SK. Intermittent large deviation of chaotic trajectory in Ikeda map: signature of extreme events. Chaos: an interdisciplinary. J Nonlinear Sci 2019;29(4):043131.
[41] Sataev IR, Stankevich NV. Cascade of torus birth bifurcations and inverse cascade of Shilnikov attractors merging at the threshold of hyperchaos. Chaos 2021;31(2):023140.
[42] Stankevich N, Kazakov A, Gonchenko S. Scenarios of hyperchaos occurrence in 4D Rössler system. Chaos 2020;30(12):123129.
[43] Gonchenko SV, Turaev DV, Shilnikov LP. Dynamical phenomena in multi-dimensional systems with a non-rough Poincare homoclinic curve. Russian Acad Sci Dokl Math 1993;47(3):410–5.
[44] Mirá C. Determination pratique du domaine de stabilité d'un point d' équilibre d'une récurrence non linéaire du deuxiéme ordre variables réelles. In: Comptes Rendus Acad. Sc. Paris, Série A. 261(2); 1964. p. 5314–7 [in French].
[45] Shykhmamedov A, Karatetskaia E, Kazakov A, Stankevich N. Hyperchaotic attractors of three-dimensional maps and scenarios of their appearance. Nonlinearity 2023. https://doi.org/10.48550/arXiv.2012.05099.